The effect of storms on the Antarctic Slope Current and the warm inflow onto the southeastern Weddell Sea continental shelf

Vår Dundas[1], Kjersti Daae[1], Elin Darelius[1], Markus Janout[2], Jean-Baptiste Sallee[3], and Svein Østerhus[4]

[1]Geophysical Institute, University of Bergen and the Bjerknes Centre for Climate Research, Alleg. 70, Bergen, Norway
[2]Alfred-Wegener-Institute Helmholtz Centre for Polar and Marine Research, Am Handelshafen 12, D-27570 Bremerhaven, Germany
[3]Sorbonne Université/CNRS/IRD/MNHN, LOCEAN-IPSL, Laboratoire d'Océanographie et du Climat: Expérimentation et Approches Numériques, Paris, France
[4]NORCE Norwegian Research Centre and Bjerknes Centre for Climate Research, Nygårdsgt 112, Bergen, Norway

Correspondence: Vår Dundas (var.dundas@uib.no)

Abstract. The southern Weddell Sea and the Filchner Ice Shelf cavity are locations of dense bottom water production and are thus connected to the global climate system. However, it has been suggested that increased heat transport from the deep ocean onto the continental shelf and towards the ice cavities would disrupt the dense water production and increase ice shelf melt rates. Processes that affect the southward heat transport are, therefore, important to understand. Sudden strong westward
5 ocean surface stress events – "storms" – are suggested to drive enhanced southward transport of modified Warm Deep Water across the continental shelf in the Filchner Trough region in the southeastern Weddell Sea. We use a mooring network with up to four year long mooring records from the region to investigate how the ocean circulation responds to storm events. We find that about 70% of the events that last longer than four days, have a cumulative westward stress increase larger than $0.4\,\mathrm{N\,m^{-2}\,day^{-1}}$, and a maximum stress above $0.25\,\mathrm{N\,m^{-2}}$ leads to a significant increase in the speed of the Antarctic Slope
10 Current (ASC) just upstream of Filchner Trough. Roughly one-third of the identified storm events cause an increased southward current speed on the shelf. At the southernmost mooring, 76°S, storm responses are observed mainly during the latter part of the record (mid-2019 to early 2021). This interannual variability in storm response indicates a potential dependency on background hydrography and circulation that remains to be fully explained. This study highlights the potential importance of storms for southward heat transport towards the Antarctic ice shelves. Warm water that is present on the continental shelf during a storm
15 will likely be pushed southward by the enhanced circulation, increasing the southward heat transport and the likelihood that it reaches the ice shelf front before the heat is lost to the atmosphere during winter.

1 Introduction

Sudden strong ocean surface stress events – "storms" – are suggested to cause enhanced southward transport of modified Warm Deep Water (mWDW, ~ -1.5°C to 0.0°C, Nicholls et al., 2009) across the continental shelf in the southeastern Weddell Sea
20 (Darelius et al., 2016; Dundas et al., 2024), which is today characterized as a cold, dense shelf region (Thompson et al., 2018). Southward intrusions of mWDW, originating from the open ocean north of the continental shelf break (Ryan et al., 2016),
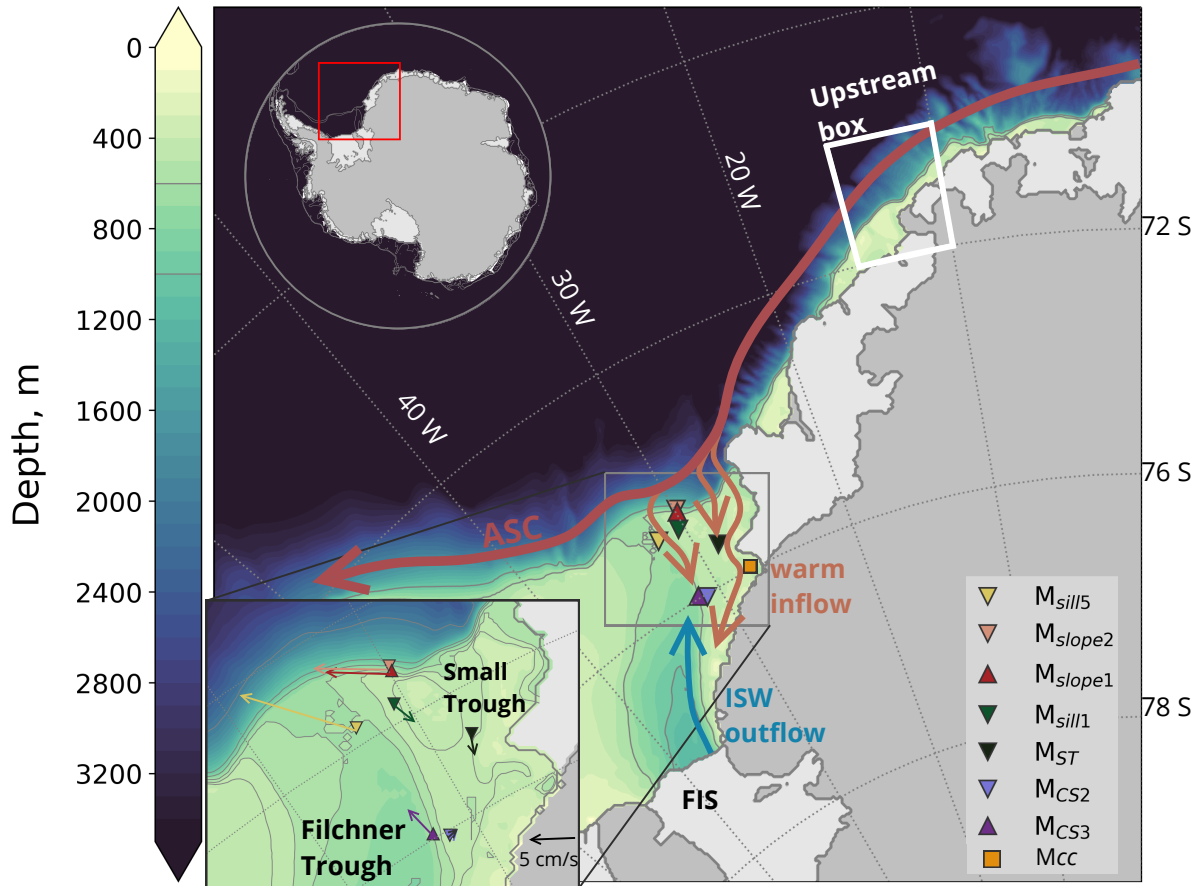
Figure 1. Bathymetry, the ice shelves, and the ice sheet from Bedmap2 (Fretwell et al., 2013) with selected depth contours (gray lines on map and colorbar). The red box in the inset in the upper left corner indicates the study region. The mooring locations of M_{slope2}, M_{slope1}, M_{sill1}, M_{ST}, M_{sill5}, M_{CS3} and M_{CS2} are indicated by colored markers. The orange square (M_{CC}) indicates the location of a mooring that captured the Coastal Current from 2003 to 2004 (Daae et al., 2018; Nicholls, 2005). The inset in the lower left corner zooms in on the mooring locations and shows their vertically averaged current, with a black scale arrow of 5 cm s^{-1}. The white box ("Upstream box") is used for estimates of the ocean surface stress. Filchner Trough, the Small Trough, and Filchner Ice Shelf (FIS) are labeled, and the main currents are indicated. The ASC (red arrow) and the Coastal Current and warm inflow through Filchner Trough (orange arrows) are based on Nicholls et al. (2009), while the northward ISW (blue arrow) is based on Darelius et al. (2014).

are mostly limited to the summer season when the thermocline is shallow (e.g., Darelius et al., 2024b; Årthun et al., 2012). These intrusion of mWDW onto the continental shelf extends up to roughly 300 m depth, creating a thick layer of warm waters below the cold surface waters (e.g., Steiger et al., 2024; Årthun et al., 2012). The warm water then propagates southward

25 throughout fall, reaching 76°S, roughly halfway south to the Filchner Ice Shelf, several months later (Steiger et al., 2024; Ryan et al., 2017). Darelius et al. (2016) suggested storms as a driver of particularly far-reaching intrusions of warm water as they observed coinciding events of strong, short-lived anomalies in wind speed and enhanced ocean currents carrying mWDW southward along the eastern flank of the Filchner Trough toward the Filchner Ice front. In model studies, mWDW entering the Filchner Ice Shelf cavity along this path has been suggested to potentially cause the system to change into a warmer regime with

30 dramatically increased melt rates in the future (Hellmer et al., 2012, 2017). Enhanced basal melt affects sea level, hydrography on the continental shelf, deep water production, and, by extension, the global climate (Orsi et al., 1999; Marshall and Speer, 2012; Jacobs, 2004). Given these implications, this study aims to deepen our understanding of how sudden strong wind events affect the circulation and the transport of heat in the region.

A strong horizontal density gradient known as the Antarctic Slope Front (ASF), separates the cold shelf waters from the

35 warm water of the open ocean (e.g., Gill, 1973; Jacobs, 1991; Thompson et al., 2018). In the Weddell Sea, the ASF relaxes during summer due to weaker wind and stronger surface stratification (Hattermann, 2018; Daae et al., 2017) and allows warm water to access the continental shelf (e.g., Årthun et al., 2012; Ryan et al., 2017; Steiger et al., 2024). The persistent westward wind field (Hazel and Stewart, 2019) and the ASF support the strong westward Antarctic Slope Current (ASC, e.g., Thompson et al., 2018; Gill, 1973). The ASF and the ASC thus make up a strongly coupled system. The strong easterlies during winter

40 lead to Ekman convergence and coastal downwelling that will act to steepen the ASF and sustain a strong ASC (Thompson et al., 2018). The winds are generally weaker during summer while the surface stratification is stronger (Hattermann, 2018). This allows for a relaxation of the ASF and a weaker ASC. However, the relationship between the wind, the ASF, and the ASC is different on short time scales.

Sudden strong easterlies increase the Sea Surface Height (SSH) slope through Ekman transport towards the coast, which

45 enhances the barotropic component of the ASC. This is the main mechanism by which storms are suggested to enhance the heat transport towards the Filchner Ice Shelf cavity: a barotropically increased ASC due to storm-driven enhanced SSH-slope accelerates the circulation on the shelf and moves warm waters already present on the continental shelf faster towards the south (Darelius et al., 2016; Dundas et al., 2024). The water column on the shelf is homogenized during winter and all heat is lost to the atmosphere (Ryan et al., 2017), so the warm inflow must traverse the continental shelf during the summer season if it is to

50 reach the ice shelf cavity.

The deep Filchner Trough crosscuts the southeastern Weddell Sea continental shelf and acts as a southward gateway for mWDW towards the Filchner Ice Shelf cavity in the south (Fig. 1). At the mouth of Filchner Trough, the ASC bifurcates as the diverging isobaths steer a small branch of the current southward along the eastern flank of the trough (leftmost orange arrow in Fig. 1, e.g., Nicholls et al., 2009; Foldvik et al., 1985). Part of this southward-flowing current recirculates on the

55 sill and joins the northward flow of Dense Shelf Water (DSW, Daae et al., 2017; Foldvik et al., 2004). The remainder of the current continues south (e.g., Daae et al., 2017; Steiger et al., 2024), advecting warm mWDW southward along the eastern

flank of Filchner Trough and onto the continental shelf east of the trough (e.g., Ryan et al., 2017; Darelius et al., 2016; Daae et al., 2020). Intrusions of mWDW have also been observed further east as indicated by the two easternmost arrows in Fig. 1 (Steiger et al., 2024; Nicholls et al., 2009). In addition to the effect of the shelf break processes, this overall circulation in

60   Filchner Trough is affected by large scale variability in the ice shelf cavity such as shifts between the "Berkner" and "Ronne" modes of Ice Shelf Water production (ISW, below-freezing temperatures, e.g., Foldvik et al., 2004), where the "Ronne"-mode is connected to enhanced ISW outflow (Hattermann et al., 2021; Janout et al., 2021).

Numerical experiments performed in an idealized setup of the Regional Ocean Modeling System (ROMS, Shchepetkin and McWilliams, 2009) support the hypothesis that storms can enhance the southward heat transport as long as warm water is

65   present on the continental shelf and the storm is sufficiently strong and long-lasting to cause a substantial increase in the circulation (Dundas et al., 2024). Previous mooring observations from the region, however, do not consistently show a relationship between southward transport and strong winds at 76°S (Ryan et al., 2017).

In this paper, we investigate how the circulation responds to strong wind forcing using up to four-year-long records of concurrent mooring data from the upper continental slope, the Filchner Trough sill, and the continental shelf east of the trough.

70   We investigate the conditions during which strong ocean surface stress drives enhanced currents over the slope and into Filchner Trough. We first present a case study that shows the current's potential response to a sudden, strong ocean surface stress event. Secondly, we look at composites of the response to the strong ocean surface stress events as well as the average atmospheric conditions during these events. We then consider why some events cause strongly enhanced currents while others do not, and lastly, discuss a shift in hydrographic conditions and circulation that occurred during 2019, which appears to have impacted

75   the potential of the ocean surface stress to cause strongly enhanced circulation on the southern part of the shelf. We, thus, provide new insights into the importance of storm events for the ASC and the southward heat transport in the ~~Filchner~~ region and describe the nuances of why and when strong ocean surface stress events cause enhanced circulation in the region.

2 Data and methods

2.1 Mooring records

80   We analyze velocity, temperature, and salinity records from ~~seven~~ moorings in the Filchner Trough region in the Southeastern Weddell Sea (Fig. 1). The mooring names indicate their geographic location: M_{slope1} (Darelius et al., 2024a) and M_{slope2} (Darelius et al., 2023b) were positioned on the ~~upper~~ part of the continental slope and captured the ASC just upstream of Filchner Trough. M_{sill5} (Østerhus, 2024) and M_{sill1} (Steiger et al., 2024) captured the outflow and inflow on the Filchner Trough sill, respectively. M_{ST} (Steiger et al., 2024) was located in the trough just east of Filchner Trough, which we refer to

85   as the "Small Trough" (Fig. 1). M_{CS2} (Darelius et al., 2023b) and M_{CS3} (Steiger et al., 2024) were located on the continental shelf on the eastern flank of Filchner Trough. The mooring locations are shown in Fig. 1, and their deployment details are given in Fig. 2 and Table 1. The mooring records span a varying period between 2017 and 2021, but their velocity records overlap for at least 20 months (Fig. 4).
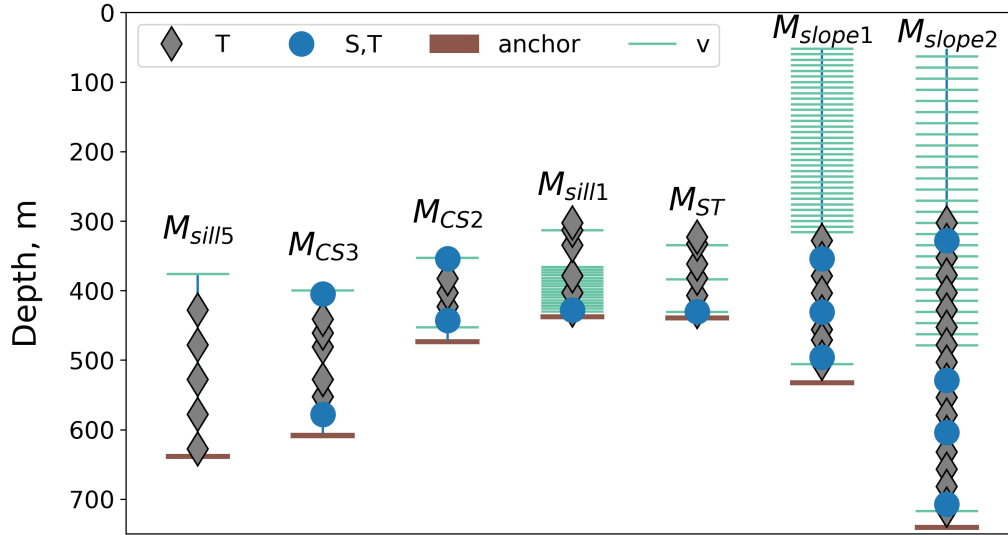
Figure 2. Sketch of the moorings indicating the depth of available observation records. Horizontal turquoise lines indicate measurements of velocity. Frequent turquoise lines indicate ADCP measurements (M_{sill1}, M_{slope1}, and M_{slope2}). The brown horizontal line indicates the bottom.

We rotate the coordinate system at each mooring to align with the mean flow direction (see Fig. 1), where a negative sign indicates current speed in the mean flow direction since the mean flows are roughly westward (M_{slope1} and M_{slope2}) and southward (M_{sill1} and M_{ST}). M_{CS2} and M_{sill5} are the exceptions: at M_{sill5} a positive sign indicates current in the main flow direction since the main flow direction is roughly northward, and at M_{CS2} we align the coordinate system with the local isobaths (see Fig. 1) with a negative sign indicating flow towards the southwest.

All analyses are carried out using hourly mean velocity records: we interpolate the data from moorings M_{slope2}, M_{CS2} and M_{sill5}, which are on a two-hourly frequency, onto hourly time steps.

For moorings with high vertical resolution (M_{slope1}, M_{slope2}, M_{ST}), we base the analysis on depth-averaged currents. At M_{slope1} and M_{slope2}, the data quality of the upper bins is poor during winter (due to too few scattering particles), and we've discarded levels with less than 43% data coverage at M_{slope1} and M_{slope2}. Data gaps shorter than six hours are filled by linear interpolation. The bottom sensor (Fig. 2) at both these moorings, which had the highest data quality and the strongest current (Darelius et al., 2024a), stopped recording in June 2019. For moorings with varying record lengths at different depths (M_{sill1}), we use the data with the longest time series, and for the moorings with strong vertical variability (M_{CS2}), we use the depth with the highest velocities.

We present temperature and salinity as conservative temperature, Θ, and absolute salinity, S_A, following TEOS-10, unless otherwise stated. We use the Gibbs seawater package for Python in conversions (McDougall and Barker, 2011).

Table 1. Overview of the moorings. The indicated significance values for storm response are negative for all moorings except M_{sill5} because their main observed flow directions are westward or southward. The significance value at M_{sill5} is positive because the main flow direction is northward. No significance value is indicated for M_{CS3} because this mooring is dominated by northward flowing ISW and not used in the storm response analysis.

Mooring name	Original name	Deployment/ Recovery	Lon/ Lat	Bottom depth [m]	Significance value [cm s^{-1}]
M_{slope2} (UiB)	M3	24.02.2017 14.02.2021	29°54.48'W 74°33.00'S	740	-9.06
M_{slope1} (UiB)	M6	24.02.2017 13.02.2021	29°54.97'W 74°35.70'S	530	-7.64
M_{sill1} (LOCEAN)	P4	11.02.2017 15.02.2021	30°23.01'W 74°51.00'S	435	-6.01
M_{ST} (LOCEAN)	P5	09.02.2017 09.03.2021	28°38.22'W 75°23.38'S	437	-5.67
M_{sill5} (NORCE)	S2	07.02.2018 16.02.2021	31°49.84'W 74°51.32'S	636	17.75
M_{CS2} (AWI)	A253-3	05.02.2018 01.03.2021	31°01.42'W 76°02.74'S	471	-7.26
M_{CS3} (AWI)	A253-4	05.02.2018 02.03.2021	31°29.79'W 75°57.68'S	606	N/A

2.2 Atmospheric and sea ice data

We use $10\,\mathrm{m}$ wind velocity, sea ice concentration (SIC), and mean sea level pressure from ERA5 (Hersbach et al., 2023). For the maps in Figures 5 and 9, we use daily averaged output from ERA5. The anomalies of wind velocity and mean sea level pressure are referenced to monthly averaged March fields from 1990 to 2023. The sea ice concentration is referenced to the monthly climatology (average past 30 years), linearly interpolated onto daily values.

To estimate the ocean surface stress, $\overrightarrow{\tau}$, we average the three-hourly 10m wind and SIC over a region upstream of Filchner Trough ("Upstream box", Fig. 1). We chose this region because upstream wind forcing has been found to drive variability in circulation in this and similar regions on longer time scales (Daae et al., 2018; Lauber et al., 2023). Since we investigate the effect of sudden strong ocean surface stress events, we make the Upstream box relatively small – we want to avoid smoothing out maximum stress values. To estimate the sensitivity to the choice of box, we estimate the correlation between the wind speed averaged over the Upstream box and the wind speed in the surrounding regions (Fig. A1). The correlation is high in a large region surrounding the Upstream box, so we infer that the sensitivity to the exact choice of the box is small.

Ocean surface stress is estimated following Dotto et al. (2018), which estimates the air-ocean stress and ice-ocean stress separately and then combines these stresses as fractions of the SIC as follows:

$$\overrightarrow{\tau} = \alpha \overrightarrow{\tau}_{ice-water} + (1-\alpha)\overrightarrow{\tau}_{air-water}, \tag{1}$$

120
$$\overrightarrow{\tau}_{ice-water} = \rho_{water} C_{iw} |\overrightarrow{U}_{ice}| \overrightarrow{U}_{ice}, \quad \text{and} \tag{2}$$

$$\overrightarrow{\tau}_{air-water} = \rho_{air} C_{d} |\overrightarrow{U}_{air}| \overrightarrow{U}_{air}, \tag{3}$$

$$\tag{4}$$

where α is the SIC, $\rho_{water} = 1028 \,\mathrm{kg\,m^{-3}}$, $\rho_{air} = 1.25 \,\mathrm{kg\,m^{-3}}$, $C_d = 1.25 \times 10^{-3}$ and $C_{iw} = 5.50 \times 10^{-3}$ are the drag coefficients between air and ocean and ice and ocean, respectively, and $\overrightarrow{U}_{ice}$ and $\overrightarrow{U}_{air}$ are the velocities of the ice and the
125 air.

We use sea ice motion from the Upstream box (Fig. 1). The sea ice motion data is from NSIDC (Tschudi et al., 2019a) and stored on the 25 km EASE-Grid (NSIDC, 2019). We, thus, average over the grid cells that overlap with the Upstream box and convert the data to northward and eastward components by applying a rotational matrix as described in the data set's user resources (NSIDC, 2024) to estimate the ocean surface stress.

130 The records of westward ocean surface stress are de-trended and then high-pass filtered using a fourth order $180\,\mathrm{day}$ Butterworth filter to remove seasonality. We then identify storm events as periods when the cumulative stress increases monotonically for more than $12\,\mathrm{h}$ and where the total increase is at least $1.5\,\mathrm{N\,m^{-2}}$. We combine two storm events into one if they are less than $15\,\mathrm{hours}$ apart. This condition is based on idealized model results from Dundas et al. (2024), which indicates that the circulation increases throughout the storm duration and stays enhanced for a few days after the storm has passed. This means
135 that a storm that occurs shortly after another adds momentum to an already enhanced current field. With this algorithm, we disregard the shortest and weakest wind events from further analysis, as we do not expect them to cause increased circulation (Dundas et al., 2024).

We use the cumulative ocean surface stress instead of the ocean surface stress directly because of the highly variable nature of the raw ocean surface stress signal. To avoid identifying a large number of events above a chosen ocean surface stress
140 threshold a low-pass filter would have to be applied, which makes the identification of storm start and end imprecise. The benefit of our procedure is illustrated in Fig. A2a,b.

2.3 Significant storm response

We need a definition of the current's "storm response" and an algorithm to evaluate whether an increase in ocean circulation is associated with a storm event or part of the background variability. The procedure is illustrated in Fig. A2d. Prior to the
145 analysis, the current records are low-pass filtered using a fourth order Butterworth filter with a cut-off at 40h to remove shelf waves (Jensen et al., 2013) and tides.

We find that the largest current anomalies generally occur after the maximum ocean surface stress, τ_{max}. Therefore, for each storm, we estimate the increase in current strength relative to the time $(t = t_0)$ of τ_{max} (sketch in Fig. A2d). We identify the
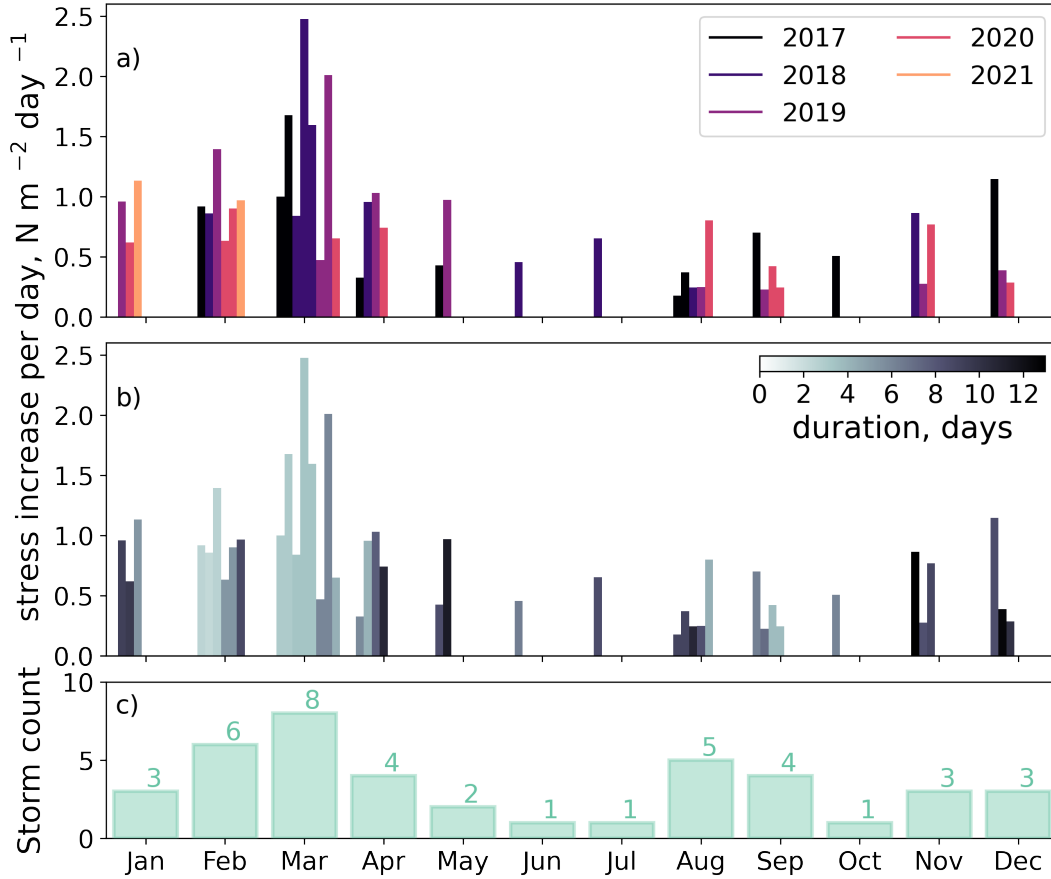
Figure 3. Distribution of storms throughout the mooring period (February 2017 to February 2021). Panels a) and b) show the increase in ocean surface stress per day for each storm on the y-axis, with a) year and b) storm duration in color. c) shows the total storm count per month.

maximum current strength during a ten-day period spanning three days before to seven days after τ_{max} ($U_{max}(t_0 - 3\,\text{days} :$

150   $t_0 + 7\,\text{days})$). This maximum current is compared with the average current two days before the ten-day period ($U_{mean}(t_0 -$ $5\,\text{days} : t_0 - 3\,\text{days})$). We define the difference between the two-day average and the maximum current as the current's "storm response" ($U_{response}$, Fig. A2d),

$$U_{response} = U_{max}(t_0 - 3\,\text{days} : t_0 + 7\,\text{days}) - U_{mean}(t_0 - 5\,\text{days} : t_0 - 3\,\text{days}) \tag{5}$$

To assess whether a storm response is significant, we compare the responses with the current increase during 10-day long,

155   50% overlapping, storm-free windows. If a storm response is higher than the 90th percentile of these non-storm periods, we consider the storm response significant (example for M_{slope1} in Fig. A2c). Each mooring consequently has its own threshold for significance due to differences in the background variability (Table 2). The number of 10-day-long storm-free periods ranges from 88 to 213.
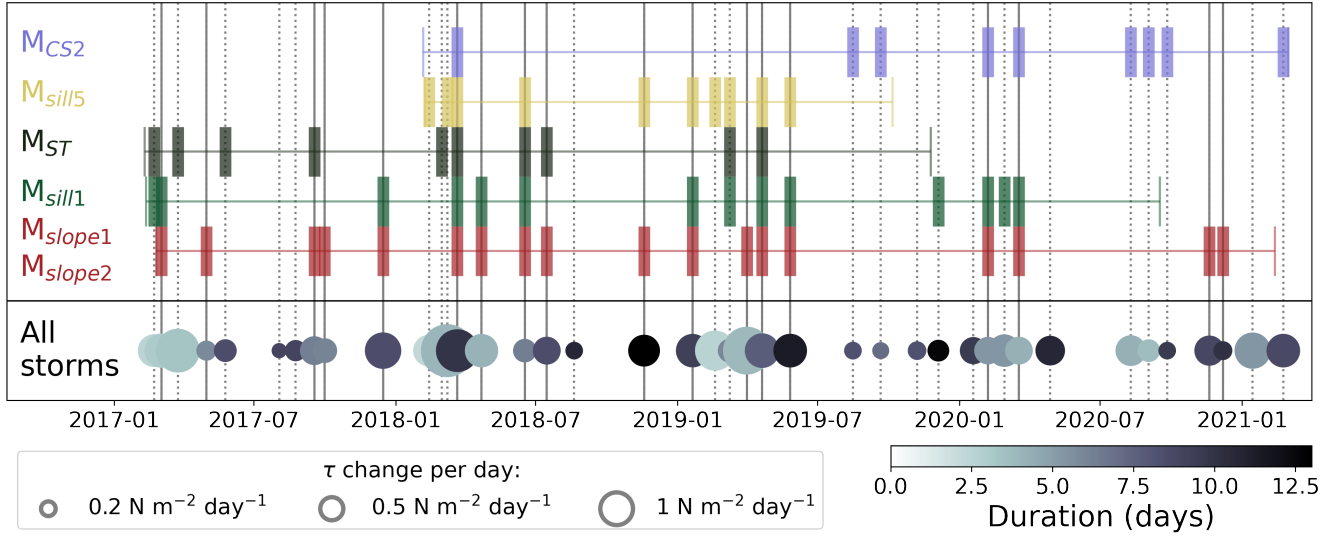
Figure 4. The duration of mooring records (horizontal colored lines) with colored vertical bars indicating a significant storm response. The vertical black solid lines indicate a significant response at both M_{slope1} and M_{slope2}, while vertical dotted lines indicate storms that do not give a significant response at M_{slope1} and M_{slope2}. The grayscale circles at the bottom indicate the duration (color) and change in ocean surface stress, τ, per day (size) for the identified storms.

2.4 Source salinity estimates

160   To estimate the arrival of the shift from Berkner to Ronne mode described by Hattermann et al. (2021) and Janout et al. (2021), we estimate the source salinity of the waters at M_{CS3} by identifying the intersection between the Gade line (Gade, 1979) and the surface freezing point in ΘS_A space (illustrated in Fig. A4). Solving the linear relationship given by Wåhlin et al. (2010) for the source salinity, S_0, gives

$$S_0 = S\left[1 + \frac{cp}{L_f}(T_0 - T)\right], \qquad (6)$$

165   where $cp = 4186$ J kg^{-1} K^{-1} and $L_f = 3.34 \times 10^5$ J kg^{-1}. By first estimating the surface freezing temperature, T_0, at the recorded salinity, S, and then using Eq. 6 to estimate the corresponding source salinity, S_0, we obtain an initial estimate of where the salinity-dependent surface freezing point intersects with the Gade line. The calculation is repeated once, replacing S by S_0 to find a new T_0 and S_0 (Fig. A4).

3   Results and discussion

We identify 41 strong wind events that we classify as "storms" between February 2017 and February 2021 (Fig. 4). The storms are spread throughout the four years, though the strongest and longest storms occur during fall (Fig. 3). All moorings consequently experience several storm events, and even the M_{sill5} mooring, which has the shortest record length (20 months), experiences 17 storms (Fig. 4). We find that while multiple storms cause a significant response in the circulation at many of the mooring locations, several storms do not (Fig. 4). Additionally, several storms cause a significant response at some of the mooring locations but not at all of them (Fig. 4).

3.1   Case study: Storm-driven circulation increase at all moorings

We select a long (10 days) and strong ($\tau_{max} = 1\,\mathrm{N\,m^{-2}}$) storm in March 2018 to provide an example of how a storm can affect the current at the mooring locations (Fig. 5a). We choose this storm because it is particularly strong and thus provides an example of how the circulation reacts to intense surface forcing. The storm response at M_{slope2} and M_{slope1} occurs directly after the maximum peak in ocean surface stress, and the current is enhanced by roughly $15\,\mathrm{cm\,s^{-1}}$ westward (Fig. 5b) for about four days. At both M_{sill1} on the eastern flank of the sill and M_{ST} in the Small Trough, the response is significant, although it ~~lasts~~ shorter (1-2 days, Fig. 5c). At M_{sill5}, the storm causes a significant northward response (i.e. an increased outflow of DSW), although this is less evident in Fig. 5d ~~relative to~~ the other mooring locations due to the high variability during the storm period at M_{sill5}.

Figure 5. The response to the storm that started on 17-03-2018 (dotted, gray vertical lines, labeled in panel e) and reached maximum ocean surface stress, τ_{max}, on 22-03-2018 (dashed, black vertical line). Time series of a) ocean surface stress (τ) averaged over the Upstream box (black sticks), the strength of the zonal (blue) and meridional (orange) components, and the cumulative westward τ (gray, de-trended and $180\,\mathrm{day}$ high-pass-filtered). The along-flow current speed at b) M_{slope1} (red) and M_{slope2} (pale red), c) M_{sill1} (green) and M_{ST} (gray), d) M_{sill5} (yellow), and e) the current speed following the bathymetry at M_{CS2} (purple). See Figure 1 for mooring locations.

Figure 6. The atmospheric and sea ice conditions during the storm that started on the 17th of March 2018 and reached maximum ocean surface stress, τ_{max}, on the 22th of March. Anomalies of the a) mean sea level pressure with $10\,\mathrm{m}$ wind velocity vectors and b) absolute $10\,\mathrm{m}$ wind speed averaged ± 3 days of τ_{max} relative to the average March field (1990-2023). c) SIC averaged over the two days before the storm starts relative to the SIC climatology (past 30 years). d) Sea ice movement (Tschudi et al., 2019b) averaged ± 3 days of τ_{max}. White regions indicate missing data or no sea ice. In a,b), the Upstream box and the region shown in c,d) are indicated, and in c,d), the $1000\,\mathrm{m}$ and $600\,\mathrm{m}$ isobaths are indicated by gray lines (Fretwell et al., 2013). All SIC, pressure, and $10\,\mathrm{m}$ wind data are from ERA5 (Hersbach et al., 2023).

170   At M_{CS2}, along the eastern flank of Filchner Trough at 76°S, the southward storm response reaches $10\mathrm{cm\,s}^{-1}$, and the maximum current occurs shortly after the maximum stress during the storm (Fig. 5e).

    This storm, which gives a clear current response all the way south at M_{CS2}, is caused by a large low-pressure system positioned over the southern Weddell Sea (Fig. 5f). The cyclonic circulation of the low-pressure system hugs the coastline, creating a patch of anomalously high along-coast wind speeds stretching from roughly 30°W to 20°E (Fig. 5g). During the

175   three days before and after τ_{max}, the high wind speed builds up and dies down without an evident along-coast propagation (not shown). The average SIC on the eastern continental shelf and upstream of the trough is lower than the sea ice climatology, and the sea ice movement is relatively high over the continental shelf break (Fig. 5h,i). We hypothesize that the location and

structure of the low-pressure system are important for the resulting oceanic response. It also emphasizes the effect of upstream ocean surface stress conditions, in agreement with, e.g., Daae et al. (2018) and Lauber et al. (2023).

3.2 Composite analysis: the mean storm response

Following the case study, which provides evidence that a storm can cause both an enhanced ASC and enhanced current far south along the flank of both Filchner Trough and the Small Trough, we conduct a composite analysis of the current at the moorings during all the identified storms. We group the composites into two classes: those that give a significant response and those that do not. The composites give several consistent indications of the effect of a storm event on the circulation at the moorings.

At M_{slope2} and M_{slope1}, where we expect the strongest storm response since they are located over the slope and capture the acceleration of the ASC directly, more than half of the storms cause a significant increase in the westward current (average response: $\sim 10 \mathrm{cms}^{-1}$ westward, Fig. 4, 7c,e, and Table 2). The mean current speed during the response-giving storms is 65% higher than the record mean current at M_{slope1} and 42% higher at M_{slope2}.

The thermocline over the slope at M_{slope2}, represented by the $-1.7°$ isotherm, is only weakly pushed down (on average 30 m during the storms with a significant response at M_{slope1} and M_{slope2}, not shown). This is substantially less than the high-frequency fluctuations caused by shelf waves and tides (which is on the order of 100-200 m, Semper and Darelius, 2017; Jensen et al., 2013) and thus, depression of the thermocline caused by the storms do not substantially impede the access of warm water onto the continental shelf. Although the development of a fresh and warm surface layer has been suggested to "protect" the (deeper) ASF from the influence of wind during summer (Hattermann, 2018), there is no substantial difference between the storm's short-term effect on the thermocline in summer and winter.

Both within the inflow on the sill and in the Small Trough (M_{sill1} and M_{ST}) more than one-third of the storms cause a significantly increased southward current (average response: $7.8 \mathrm{cms}^{-1}$ and $7.2 \mathrm{cms}^{-1}$, Fig. 7a,d, Table 2). At M_{sill1}, all events with a significant response occur between December and June, i.e., from late spring to early winter (Fig. 4) although just 66% of all the storms occur during these months (Fig. 3c). The same is true for 80% of the events that cause a significant storm response at M_{ST} (Fig. 4).

Within the observed ISW outflow, at the location of M_{sill5}, periods of strong along-slope wind co-vary with enhanced overflow on monthly (Daae et al., 2018) time scales. Idealized numerical experiments (Dundas et al., 2024) also suggest that storms can drive an adjustment of the SSH across a trough, thus connecting the southward inflow and the northward outflow. This is similar to the situation described by Morrison et al. (2020) and observed by Darelius et al. (2023a), where the downslope flow of DSW along a canyon or ridge causes an SSH anomaly that drives an upslope flow of WDW east of the corrugation. We, therefore, expect that the storms induce enhanced outflow (i.e. northward flow) at M_{sill5}. While the mean current and the high-frequency variability of the outflow at M_{sill5} are higher than at the other moorings, the average significant storm response is northward flow at $16 \mathrm{cms}^{-1}$ (Fig. 7e).

Just as at the other moorings close to the shelf break, there is a tendency for a seasonal signal in the significant storm response at M_{sill5}. Here, 90% of storm responses occur between December and June. This agrees with the seasonality in the observed
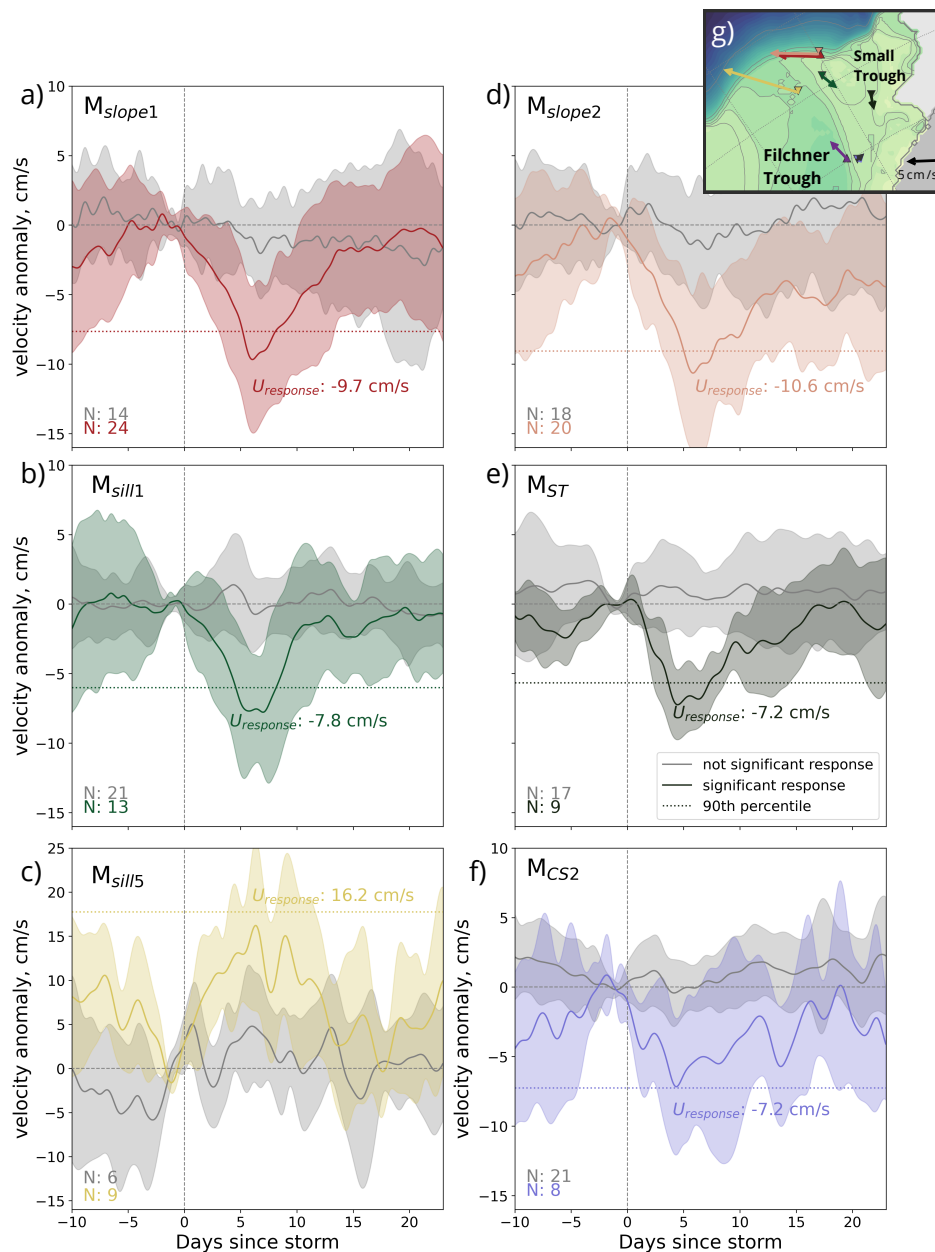
Figure 7. The composite average storm response at a) M_{slope1}, b) M_{sill1}, c) M_{sill5}, d) M_{slope2}, e) M_{ST}, and f) M_{CS2}. In each panel, the average response (line) and the standard deviation (area) to storms that give a response (increased velocity anomaly) are shown in color, while the average current following storms that do not give a significant response is shown in gray. The legend in e) is common for all panels. The threshold for significance (see Table 1, horizontal colored, dotted lines) and the number of events (N) included are indicated. Since these composites are estimated individually for each mooring, the specific storms driving the response shown are not always the same (see Fig. 4). Day zero is the start of the period used to estimate $U_{response}$, i.e., $t_0 - 3\,days$ (see Fig. A2). We only include the events where we have data for the 33 days shown in each panel. Events close to the start or end of each mooring period are consequently not included in this figure. The map in the upper corner (g) shows the mooring locations and their mean current directions.

Table 2. Overview of parameters from the composite analysis of storm response ($U_{response}$: Equation 5 and Fig. A2d) at the moorings. The % of response-giving storms is estimated relative to the storms occurring during each moorings record.

Mooring name	Average anomaly $U_{response}$ [cm s^{-1}]	Response-giving storms, N/total
M_{slope2}	-11 ± 6	21/39 (54%)
M_{slope1}	-10 ± 5	25/39 (64%)
M_{sill1}	-8 ± 4	14/34 (39%)
M_{ST}	-7 ± 3	10/28 (36%)
M_{sill5}	16 ± 10	10/17 (59%)
M_{CS2}	-7 ± 5	9/31 (29%)

relationship between wind and the overflow on the sill in 2009 (Daae et al., 2018). We note that the M_{sill5} mooring stopped recording current velocities after roughly 1.5 years. Thus, 17 storm periods are captured within this mooring period, which leaves few samples on which to base our conclusions regarding the seasonality in response at M_{sill5}. However, this location

215   displays a high fraction of significant storm response events (59% vs. 53% at M_{slope1} and M_{slope2}, 41% at M_{sill1}, and 35% at M_{ST} during the same period, Fig. 4).

    The ocean surface stress increase per day is largest in summer and fall (Fig. 3). Strong and long storm events are expected to cause the largest current response (Dundas et al., 2024), and thus, the seasonality in storm intensity likely contributes to the seasonality in storm response at M_{sill1}, M_{ST}, and M_{sill5}. The seasonality could also be linked to the seasonal signal in the

220   strength and the baroclinicity of the current at M_{slope1} and M_{slope2}, which are both strongest during fall and winter (Darelius et al., 2024a). However, we find that the storm response at M_{slope1} and M_{slope2} does not appear to depend on the baroclinicity prior to the storm (not shown). The enhanced current during winter (Darelius et al., 2024a) could, however, cause a larger overshoot at the mouth of the trough (Daae et al., 2017), preventing the storm signal from propagating southward along the trough and reaching M_{ST}, M_{sill1}, and M_{sill5}.

225   At the southernmost mooring location, at M_{CS2} along the eastern flank of Filchner Trough, 29% of the storms cause a significant response (Fig. 4). The average southward flow anomaly during these events is $7.2 \, \text{cm} \, \text{s}^{-1}$ (Fig. 7c). The fact that significant storm responses are recorded at this location highlights the potential for storms to increase the heat transport towards Filchner Ice Shelf in the south. If warm water is present on the continental shelf during a response-giving storm, this warm water will likely be pushed southward as observed by Darelius et al. (2016). However, it will not necessarily reach the mooring

230   during the storm event due to the relatively long background advection time scales (5-9 weeks) from the continental slope to 76°S Steiger et al. (2024).

3.3   Atmospheric conditions: storm response or not?

The composite analysis of the current's response to storm events shows that while many storms drive a significant increase in the current at the various mooring locations, several storms do not. We note, however, that the results are sensitive to our choice of

235   significance threshold. When we lower the threshold for significance from the 90th to the 70th percentile of current increase, the number of storms that give a significantly enhanced current at both slope-moorings (M_{slope1} and M_{slope2}) increases from 46% to 74% (Fig. 10a). At M_{CS2}, two storms in 2018 become significant when lowering the threshold (Fig. 10a). This emphasizes that the storms we identify as not giving a significant current response may still influence the circulation although we do not resolve this response with our method due to the high background variability.

240   Most storms that cause a strong response on the Filchner Sill and in the Small Trough also enhance the ASC and show a significant response at the slope moorings (Fig. 4). Since the records from the slope moorings are the longest, we focus on these when investigating the atmospheric conditions that give a significant storm response.

    The response of the ASC to a storm depends on the storm duration, the ocean surface stress increase during the storm, and the maximum stress (Fig. 8). We find that 70% of storms that are i) longer than four days, ii) have a stress increase larger than

245   $0.4\,\mathrm{N\,m^{-2}\,day^{-1}}$, and iii) have ~~higher~~ maximum stress than $0.25\,\mathrm{N\,m^{-2}}$, give a significant increase in the ASC speed during 2017 to 2021.

    Periods of low ocean surface stress correspond to periods of low variability in the ASC (not shown) and storms occurring during this period are generally without significant storm responses in the ASC. Low ocean surface stress periods generally occur during mid-winter (not shown). We, therefore, hypothesize that the mid-winter sea ice pack dampens the momentum

250   transfer into the ocean. This dampening might be caused by a highly compact sea ice cover (Martin et al., 2014), low rigidity (Steele et al., 1997), low surface and bottom roughness (Martin et al., 2016; Tsamados et al., 2014), or a combination of these factors. When the SIC approaches 100%, the total ocean surface stress is nearly entirely determined by the momentum transfer from the sea ice to the ocean (Eq. 4). Within these periods, the weakest ice-ocean stress is, thus, when the sea ice is the least mobile, which also occurs during mid-winter (not shown). During mid-winter, the mooring locations ~~consequently~~ experience

255   low total ocean surface stress, weak storms (Fig. 3), and weak air-sea momentum transfer. Consequently, there are both few storms (34% of storms, Fig. 3c) between July and November and few (28%) significant storm response events within the ASC (Fig. 4).

    Zooming out to large-scale atmospheric patterns, the low-pressure systems that significantly enhance the ASC are generally deeper and more structured than those that do not enhance the ASC (Fig. 9a,e,i). The wind speed is strongly enhanced along

260   the coast upstream of the study area (Fig. 9b,f,j), and the sea ice movement is high (Fig. 9d,h,l). Prior to the storm events, the SIC is also, on average, lower compared to the climatology when there is a response than when there is not (Fig. 9c,g,k). We hypothesize that the relatively low SIC, high sea ice mobility and strongly enhanced wind along the coast upstream of the southeastern Weddell Sea favor efficient momentum transfer into the ocean. This enhances the cross-slope SSH and results in overall enhanced ASC and on-shelf circulation. This suggestion is ~~supported by~~ the ~~same~~ patterns occurring during the case

265   study (Fig. 5f-i).

3.4   A shift in mid-2019

At M_{CS2}, along the eastern flank of Filchner Trough at 76°S, there is an apparent shift in storm response during 2019 (Fig. 10a). Before July 2019, only one storm event causes a significant storm response at M_{CS2}. After July 2019, 50% of the storms cause a
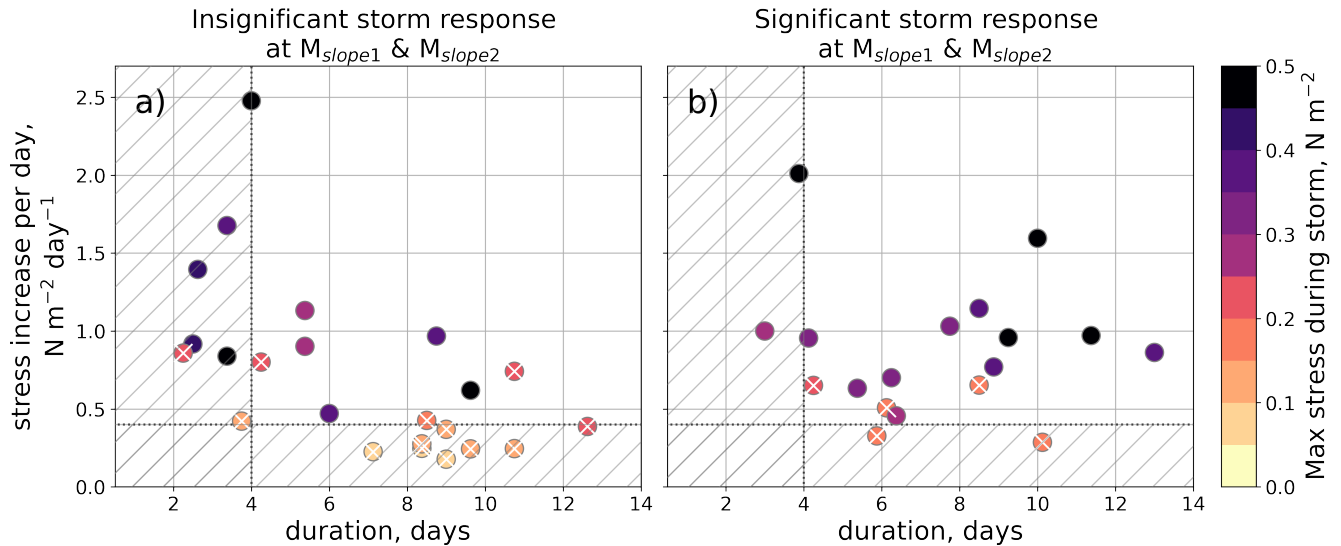
Figure 8. Scatter plots of storm duration and ocean surface stress increase per storm day, colored by the corresponding τ_{max}. The storms that do not induce a significant response at M_{slope2} and M_{slope1} are shown in panel a), and those that do are in panel b). The hatched area indicates a duration shorter than four days and/or a stress increase smaller than $0.4\,\mathrm{N\,m^{-2}\,day^{-1}}$. White crosses mark storms with $\tau_{max} < 0.25\,\mathrm{N\,m^{-2}}$.

significant storm response (Fig. 10a). Along the slope, there is a similar, but opposite, tendency towards fewer significant storm
270   response events after July 2019 (Fig. 10a). While we cannot rule this out as a coincidence, these results indicate that while all
locations are susceptible to storm-driven enhanced along-flow currents, i) the potential for a significant storm response appears
to depend on conditions that vary interannually and ii) a storm response at M_{CS2} is not necessarily driven by an enhanced ASC
that then translates southward along Filchner Trough, i.e., a storm does not necessarily enhance the circulation over the full
domain, contrary to suggestions by the idealized numerical simulations in Dundas et al. (2024).

275   Similar shifts in the response to wind forcing (correlation on monthly time scales) from one year to another were observed
within the Antarctic Coastal Current (M_{CC}, mooring location shown in Fig. 1) and on the sill (slightly further east than M_{sill5})
by Daae et al. (2018). These shifts were associated with shifts in the average wind direction and its strength along the coast
upstream of Filchner Trough: When the wind had a northwestward component and the windspeed was low, correlation with
the current weakened. We do not observe a substantial change in the direction of the mean ocean surface stress before and after
280   mid-2019 (not shown), and while there is a reduction in the variability and average speed of the zonal stress, these changes are
small (Fig. A3a).

Since there is neither an apparent change in the strength nor in the duration of the storms (Fig. 4 and 3) in July 2019, we
investigate if the shift during 2019 might be caused by a change in background circulation or hydrography on the shelf. We note
that after July 2019 i) the current at M_{CS2} veers eastward (Fig. 10b), ii) the correlation between the wind and the southward
285   current at M_{CS2} shifts from negative to positive, where a positive correlation indicates that a southwestward wind corresponds
to a southward current (Fig 10c), iii) ISW starts to dominate the winter hydrography at M_{CS2} and is associated with increased
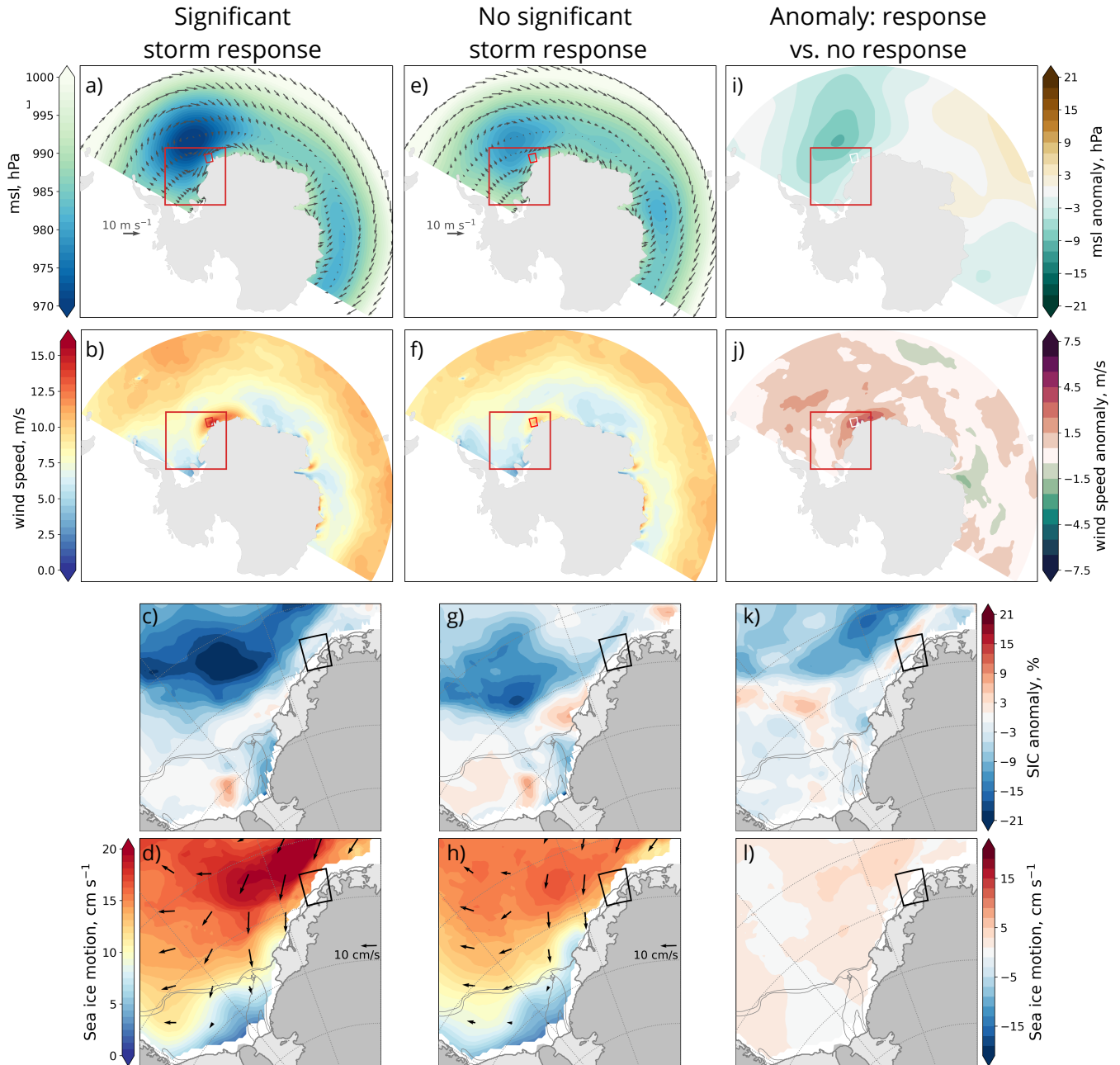
Figure 9. Composite mean atmospheric fields during storms a-d) with and e-h) without a significant storm response at M_{slope1} and M_{slope2}. The difference between the fields during storms with and without a response is shown in i-l). The first row shows the mean sea level pressure (color) and the mean $10\,\mathrm{m}$ wind (grey arrows) ± 3 days of τ_{max}. The second row shows the wind speed in color and is otherwise equal to row one. The third row shows the mean SIC anomaly (seasonal climatology removed) in a two-day-long window ending when the storm starts. The fourth row shows the speed of the sea ice motion (color) and its velocity (black arrows) in a six-day-long window centered at τ_{max}. White regions along the coast indicate missing data or no sea ice.

variability in the current (Fig. A3b), iv) at the shelf break, the warmest water is anomalously warm after mid-2019 and the seasonal cycle is disrupted (Darelius et al., 2023b), and v) the summertime SIC increases (Steiger et al., 2024).

The consistent eastward direction of the current at M_{CS2} from 2019 and onwards (Fig. 10b) is in stark contrast to the current at this location from 2014 to 2016: Then, the current had a strong seasonal cycle with a southwestward current during the warm season and west or northward during the cold season (Ryan et al., 2017). We speculate that the interannual variability in storm response might be related to variable interaction between the southward current along the eastern flank of Filchner Trough, the inflow through the Small Trough, and the Coastal Current as they all interact where the zonal extent of the continental shelf east of Filchner Trough shrinks. The complex bathymetry in the region of M_{CS2} might thus play an important role in impeding the southward signal from propagating neatly southward as it does in the model setup with idealized geometry (Dundas et al., 2024).

Since the shift is not only local but also appears to affect the storm response on the slope, it is possible that properties of the Antarctic Coastal Current (M_{CC}, Fig. 1) might affect the shift. Daae et al. (2018) observe a shift in the correlation between wind and the currents (on monthly time scales) at moorings from the Filchner Sill and the Coastal Current between 2003 and 2004 (locations indicated in Fig. 1). The Coastal Current (on the shelf) had strongest correlation with the wind in 2003, and the outflow at the sill showed the highest correlation in 2004 (Daae et al., 2018). This shift is hence similar to the shift in storm response we observed in 2019: the storm response on the shelf increases when the storm response on the slope decreases. One possible explanation could be that the storm-enhanced signal under certain conditions propagates mainly along the shelf break, causing a strong signal at the slope moorings, and in other not yet identified conditions, mainly propagates along the coast, causing a strong signal at the M_{CS2} mooring. In such a scenario, we would, however, also expect a stronger storm-response at a mooring located just east of M_{CS2} from mid-2019 onwards, but this is not the case (not shown).

In mid-2018, the circulation under the northern section of Filchner Ice Shelf changed from "Berkner mode" to "Ronne mode" (Hattermann et al., 2021; Janout et al., 2021). This means that the source waters of the ISW observed in the Filchner cavity originated from the Ronne Trough after 2018 rather than from the Berkner Shelf. We considered the possibility that the mid-2019 shift in storm response at the M_{CS2} location could be a delayed response (roughly one year lag) to this large-scale shift in circulation and hydrography. However, at M_{CS3}, which captures the northward-flowing ISW leaving the cavity, indications of the change from Berkner to Ronne mode appear already in 2018 (Fig. A3c,d). It, therefore, seems unlikely that the shift in hydrography and circulation due to the shift from Berkner to Ronne mode is a direct driver of the shift in storm-response potential at M_{CS2}. What causes the interannual shift in storm response in the southeastern Weddell Sea thus remains an open question.

4   Conclusions

We analyze a network of moorings and confirm that sudden strong ocean surface stress events – "storms" – can enhance the circulation on the southeastern Weddell Sea continental shelf. These events strengthen the westward Antarctic Slope Current (ASC), the dense outflow from the Filchner Trough, the southward flow along the eastern flank of the Filchner Trough, and the
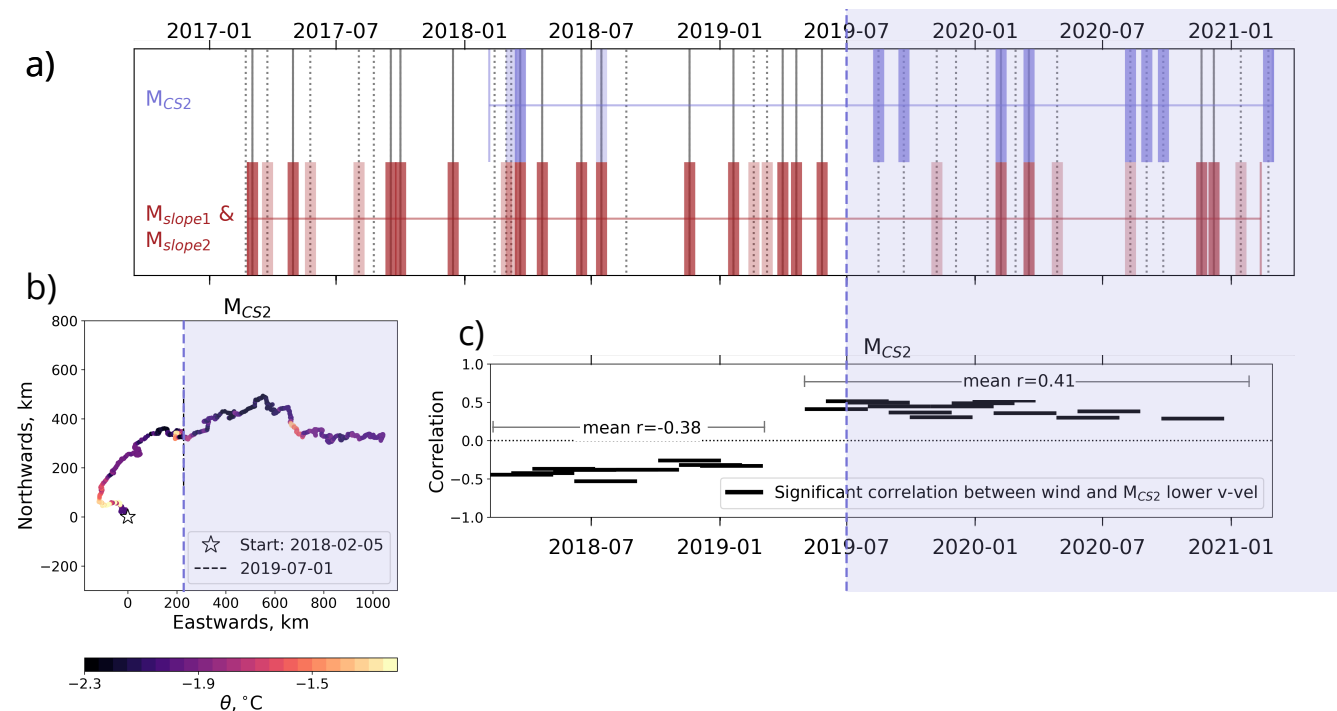
Figure 10. Indications of a shift around 2019 in the southeastern Weddell Sea shelf region. Panels a) and c) have a shared x-axis, the purple background indicates the period after July 2019, and the vertical purple dashed line indicates the 1st of July 2019. Panel a) is a simplified version of Fig. 4 showing only moorings M_{slope2} and M_{slope1} (red) and M_{CS2} (purple). The dark bars indicate significant storm responses, and the light bars show storm responses stronger than the 70th percentile of background current increase (see methods 2.3). Panel b) is a progressive vector diagram of the current at the bottom sensor of M_{CS2} colored by temperature. The temperature is based on θ and not Θ because the salinity sensor stopped recording in early 2020. The start of the time series (star) and the 1st of July 2019 (dashed line) are indicated. c) Time series from M_{CS2} of 90-day long, 33% overlapping windows of significant correlation (black bars) between the along-coast wind and the southward bottom current.

inflow through the Small Trough. These observations thus support the suggestions by Darelius et al. (2016) and the numerical experiments of Dundas et al. (2024). Our findings provide observational evidence that storms impact the southward transport of warm water in this region and suggest that this signal may extend beyond 76°S, potentially reaching the front of the Filchner Ice Shelf (Darelius et al., 2016). Since storms have the potential to enhance the southward current on the shelf, they also have the potential to push warm water southward whenever warm water is present along the eastern flank of Filchner Trough or in the Small Trough. We suggest that this is also true whenever warm water is present on the continental shelf east of Filchner Trough.

The duration of a storm, the total cumulated ocean surface stress during the event, and the maximum stress, will, to a large extent, determine whether a storm event will cause a response in the current or not. The response is, as expected, particularly

clear in the moorings on the upper part of the slope, i.e., within the ASC. 70% of the observed storms that are longer than four
330 days, have a larger stress increase than $0.4\,\mathrm{N\,m^{-2}\,day^{-1}}$, and $\tau_{max} >0.25\,\mathrm{N\,m^{-2}}$, give a significant increase in the ASC.

The enhanced circulation is, however, not so structured and steady that it can consistently be followed neatly from moorings on the slope via the sill to moorings on the shelf at 76°S. While some storms enhance the circulation in the whole region, not all storm events cause such a consistent response. This differs from the results of an idealized model Dundas et al. (2024), where storm events initiated an overall cyclonic circulation over the continental shelf east of Filchner Trough. We suggest that
335 the complex bathymetry – and potentially the interplay between the Antarctic Coastal Current and the ASC – are important factors that explain the differences between the results of the idealized model and the observations presented here.

The cause of the shift during winter 2019 from conditions that favor a storm response in the ASC to conditions that favor a storm response on the shelf at 76°S remains an open question. Other properties change around the same time, such as ~~warmer~~ temperatures along the slope (Darelius et al., 2023b), a shift from negative to positive correlation between the along-shore
340 south-westward wind and the southward current, and a shift from low to high variability in the current itself at 76°S. Following the start of 2019, Ronne-sourced ISW is consistently present at 76°S. This change is related to an overall shift from Berkner mode to Ronne mode (Hattermann et al., 2021; Janout et al., 2021) and co-occurs with a shift in the current direction at 76°S. However, as the timing of these shifts is offset by roughly half a year, we are hesitant to suggest a link between the events. These inter-annual shifts in atmospheric forcing, hydrography, and circulation emphasize the importance of ~~background~~ conditions
345 for the potential effect of storms in the southeastern Weddell Sea.

The ~~up to four-year-long~~ mooring records analyzed here give clear indications of the effect of storms on the ocean circulation in the Filchner Trough region, however, longer observational time series at the mooring sites or experiments run in a regional model setup would ~~be~~ helpful ~~to~~ understand the observed variability in storm response. ~~Based on the results presented here, a~~ regional model could also enable a realistic estimate of the potential heat transport at the ice front driven by the storm events
350 and its importance ~~relative to~~ the heat transport driven by the background flow. While this would yield additional information about the importance of storms for the basal melt of the Filchner Ice Shelf, the present study confirms the ability of storms to enhance circulation, which is the basis for bringing warm water southward towards Filchner Ronne Ice Shelf.

Data availability. The mooring data is, or will be, publicly available. M_{slope1} is available at Darelius et al. (2024), M_{slope2} at Darelius et al. (2023), M_{CS2} and M_{CS3} at Janout et al. (2022), and M_{ST} and M_{sill1} at Steiger and J.-B. (2023). M_{sill5} will be available at NMDC
355 (Østerhus, 2024). The data published before 2022 can be accessed through the Southern Ocean moored time series (south of 60°S) (OCEAN ICE D1.1) compilation (Zhou et al., 2024). The atmospheric data and sea ice concentration from ERA5 reanalysis (Hersbach et al., 2019) is available at Hersbach et al. (2023), the sea ice movement data from NSIDC is available at Tschudi et al. (2019a), and the data of bathymetry, ice shelves, and ice sheets from bedmap2 (Fretwell et al., 2013) is available at Fretwell et al. (2022).

Appendix A: Supporting figures
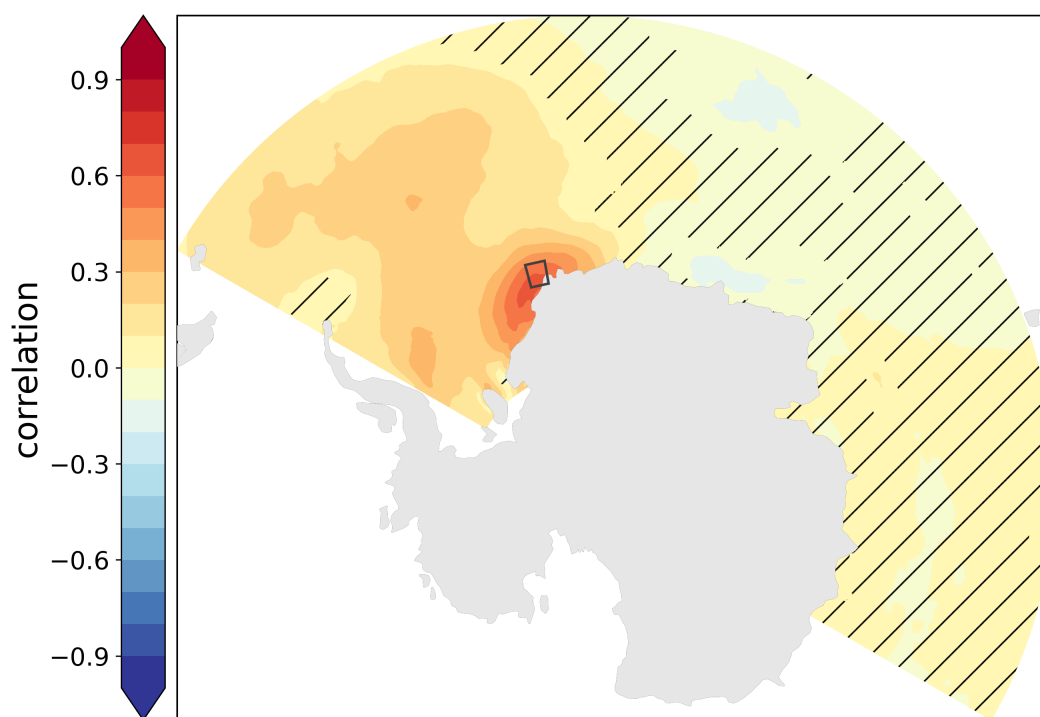
Figure A1. Correlation map of the average wind speed in the Upstream box (black rectangle) vs. the overall wind field during the observation period (2017-2021). Hatched regions indicate insignificant correlation at the 0.95 significance level.
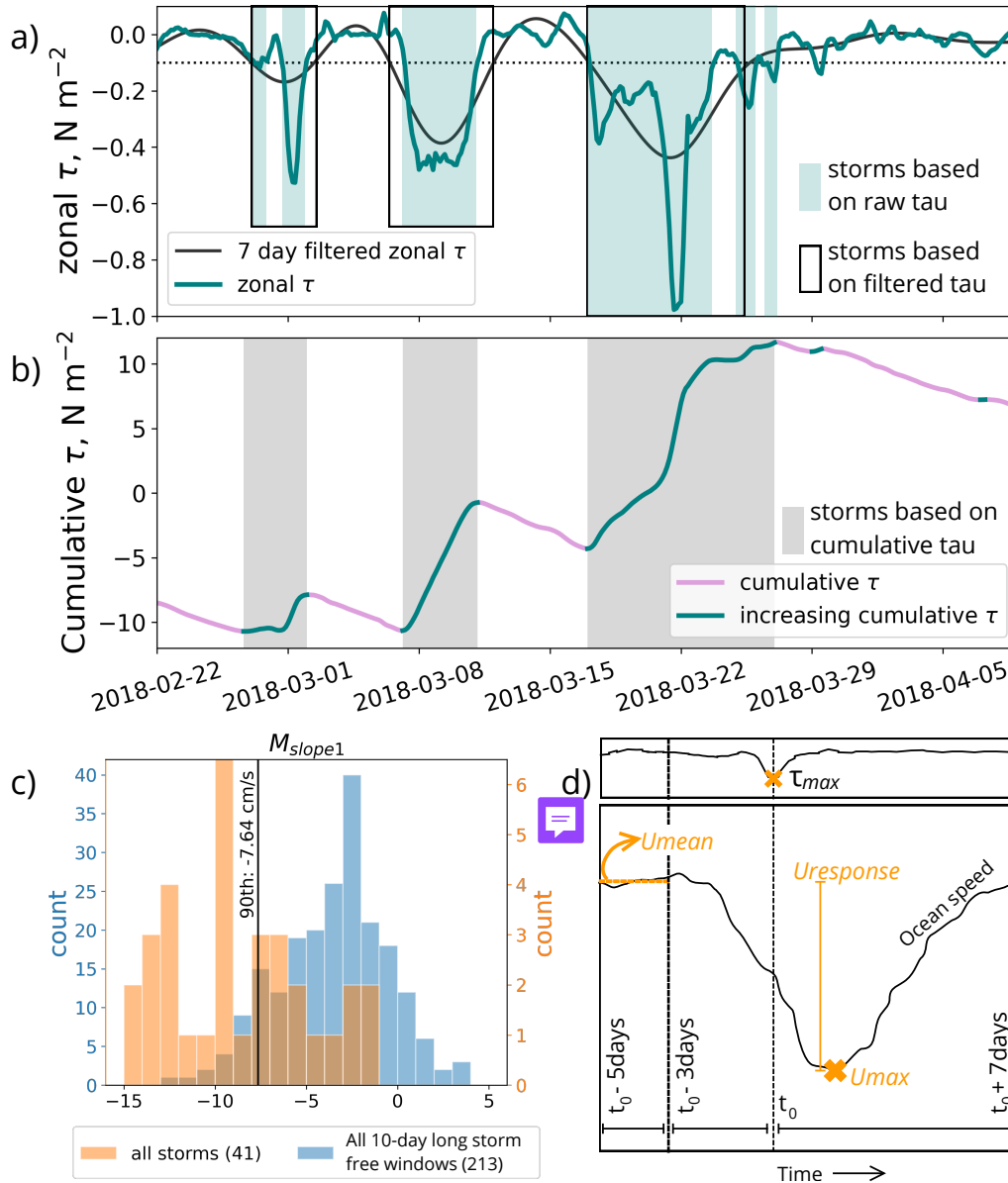
Figure A2. Example of the storm detection algorithm a,b) described in section 2.2. Time series of a) eastward ocean surface stress and b) the cumulative westward ocean surface stress. Identified storm periods based on a) the raw ocean surface stress (blue shading) and lowpass filtered ocean surface stress (black boxes) and b) based on cumulative ocean surface stress, which is the algorithm we use throughout our analysis (gray shading) are indicated. c,d) Illustrate the procedures used to determine significance and to identify $U_{response}$ as described in section 2.3. c) Histogram of $U_{response}$ (orange) and the current increase during all 10-day long storm-free windows (blue) at M_{slope1}. The 90th percentile, which is used to determine significance, is indicated (black line). d) A sketch of the procedure used to identify $U_{response}$, indicating the definition of τ_{max} in the upper sub-panel and U_{mean}, U_{max}, and $U_{response}$ in the lower sub-panel.
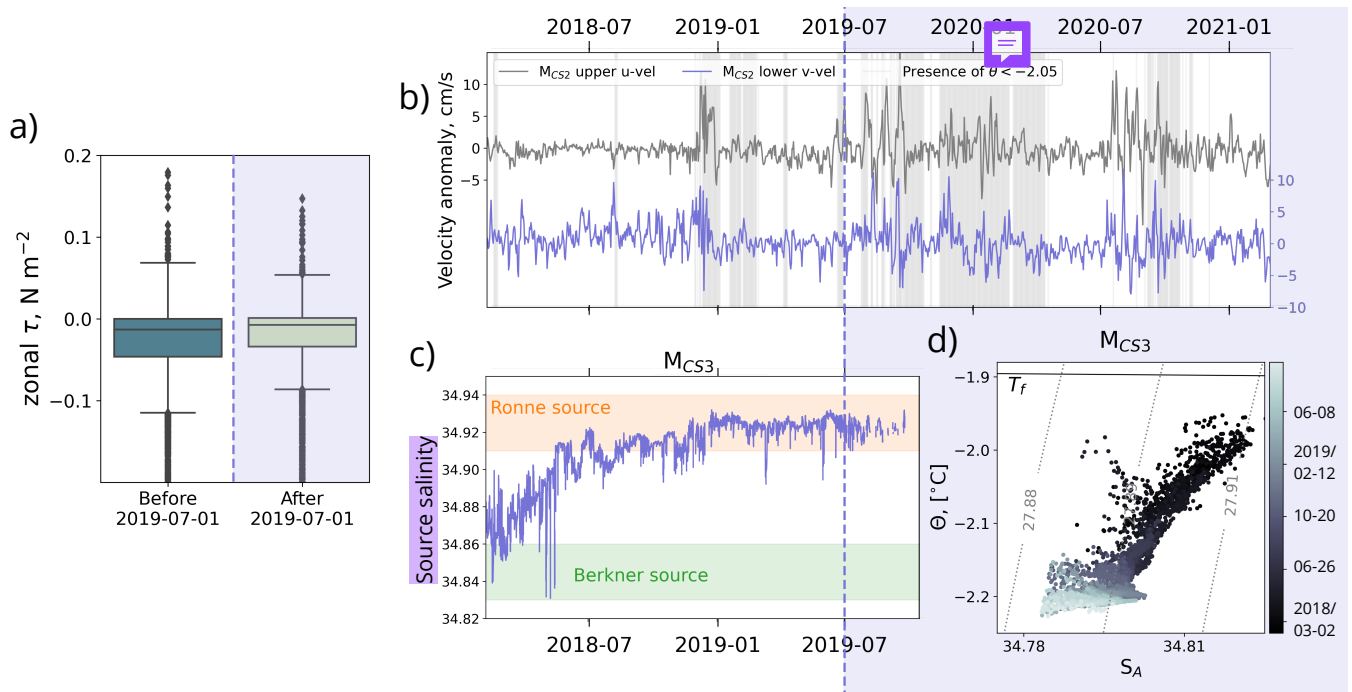
Figure A3. Additional indications of a shift around 2019 in the southeastern Weddell Sea shelf region following the same setup as Fig. 10: The purple background indicates the period after July 2019, and the vertical purple dashed line indicates the 1st of July 2019. Panel a) shows box plots of the zonal ocean surface stress before (blue) and after (green) July 2019. Panels b) and c) have a shared x-axis. b) Time series from M_{CS2} of current anomalies; eastward component at the upper sensor (gray) and the northward component at the lower sensor (purple). The gray shading indicates periods when water colder than $\theta = -2.05°C$ is present. c) Time series of the estimated ISW source water salinity at M_{CS3}. The shading indicates approximate ranges of Berkner (green) and Ronne (orange) mode source waters (Hattermann et al., 2021). d) ΘS_A-diagram from M_{CS3} colored by time, with darker colors at the start of the record. For clarity, we have omitted observations with $\sigma < 27.885 \text{kg m}^{-3}$ in panels c) and d).
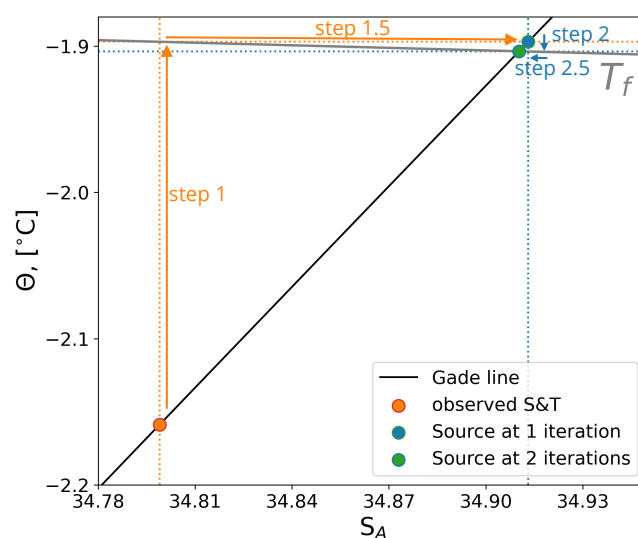
Figure A4. Illustration of the method to estimate source salinity following Equation 6. The desired value is the temperature and salinity at the intersection between the relevant Gade line and the salinity-dependent freezing point (green dot). The process is as follows: given an observed temperature and salinity pair (orange dot), the freezing point is estimated (step 1). Then, the salinity at this temperature of the Gade line is estimated (step 1.5). This completes iteration 1 and the first approximation of the source temperature and salinity (blue dot). Completing one more iteration (steps 2 and 2.5) gives a good approximation of the source water properties (green dot).

Author contributions. VD analyzed the mooring and atmospheric data, prepared the figures, and drafted the paper under the supervision of KD and ED. MJ prepared the data from the M_{CS2} and M_{CS3} moorings, JBS prepared the data from the M_{sill1} and M_{ST} moorings, SØ prepared the data from the M_{sill5} mooring, and ED prepared the data from the M_{slope1} and M_{slope2} moorings. All the co-authors read and contributed to the text and the discussion.

Competing interests. The contact author has declared that none of the authors has any competing interests.

Acknowledgements. This work was funded through the Norwegian Research Council, project numbers 267660 and 328941, and uses samples and data provided by the Alfred Wegener Institute Helmholtz-Center for Polar- and Marine Research in Bremerhaven (Grant No. AWI-PS124-03) and the European Union's Horizon 2020 research and innovation program under grant agreement N°821001 (SO-CHIC), N°820575 (TiPACCs), and N°101060452 (OCEAN:ICE). The moorings were recovered during the COSMUS expedition (PS124), and we would like to extend thanks to the officers and crew of the RV Polarstern for their work on the COSMUS cruise PS124.

References

Århun, M., Nicholls, K. W., Makinson, K., Fedak, M. A., and Boehme, L.: Seasonal inflow of warm water onto the southern Weddell Sea continental shelf , Antarctica, Geophysical Research Letters, 39, 2–7, https://doi.org/10.1029/2012GL052856, 2012.

Daae, K., Hattermann, T., Darelius, E., and Fer, I.: On the effect of topography and wind on warm water inflow—An idealized study of the southern Weddell Sea continental shelf system, Journal of Geophysical Research: Oceans, 122, 2622–2641, https://doi.org/10.1002/2016JC012541, 2017.

Daae, K., Darelius, E., Fer, I., Østerhus, S., and Ryan, S.: Wind stress mediated variability of the Filchner trough Overflow, Weddell sea, Journal of Geophysical Research: Oceans, 123, 3186–3203, https://doi.org/10.1002/2017JC013579, 2018.

Daae, K., Hattermann, T., Darelius, E., Mueller, R. D., Naughten, K. A., Timmermann, R., and Hellmer, H. H.: Necessary Conditions for Warm Inflow Toward the Filchner Ice Shelf, Weddell Sea, Geophysical Research Letters, 47, https://doi.org/10.1029/2020GL089237, 2020.

Darelius, E., Makinson, K., Daae, K., Fer, I., Holland, P. R., and Nicholls, K. W.: Hydrography and circulation in the Filchner Depression, Weddell Sea, Antarctica, Journal of Geophysical Research C: Oceans, 119, 5797–5814, https://doi.org/10.1002/2014JC010225, 2014.

Darelius, E., Fer, I., and Nicholls, K. W.: Observed vulnerability of Filchner-Ronne Ice Shelf to wind-driven inflow of warm deep water, Nature Publishing Group, pp. 1–7, https://doi.org/10.1038/ncomms12300, 2016.

Darelius, E., Daae, K., Dundas, V., Fer, I., Hellmer, H. H., Janout, M., Nicholls, K. W., Sallée, J. B., and Østerhus, S.: Observational evidence for on-shelf heat transport driven by dense water export in the Weddell Sea, Nature Communications, 14, https://doi.org/10.1038/s41467-023-36580-3, 2023a.

Darelius, E., Dundas, V., Janout, M., and Tippenhauer, S.: Sudden, local temperature increase above the continental slope in the southern Weddell Sea, Antarctica, Ocean Science, 19, 671–683, https://doi.org/10.5194/os-19-671-2023, 2023b.

Darelius, E., Janout, M. A., Fer, I., and Sallée, J.-B.: Physical oceanography and current velocity data from mooring M3 on the upper continental slope, east of Filchner Trough, February 2017 – February 2021, https://doi.org/10.1594/PANGAEA.962043, 2023.

Darelius, E., Fer, I., Janout, M., Daae, K., and Steiger, N.: Observations of the Antarctic Slope Current in the Southeastern Weddell Sea: A Bottom-Enhanced Current and Its Seasonal Variability, Journal of Geophysical Research: Oceans, 129, https://doi.org/10.1029/2023JC020666, 2024a.

Darelius, E., Fer, I., Janout, M. A., Daae, K., and Steiger, N.: Observations of the Antarctic Slope Current in the southeastern Weddell Sea: a bottom-enhanced current and its seasonal variability, Journal of Geophysical Research: Oceans, https://doi.org/10.1029/2023JC020666, 2024b.

Darelius, E., Janout, M. A., Fer, I., and Sallée, J.-B.: Physical oceanography and current velocity data from mooring M6 on the upper continental slope, east of Filchner Trough, February 2017 – February 2021, https://doi.org/10.1594/PANGAEA.964715, 2024.

Dotto, T. S., Naveira Garabato, A., Bacon, S., Tsamados, M., Holland, P. R., Hooley, J., Frajka-Williams, E., Ridout, A., and Meredith, M. P.: Variability of the Ross Gyre, Southern Ocean: Drivers and Responses Revealed by Satellite Altimetry, Geophysical Research Letters, 45, 6195–6204, https://doi.org/10.1029/2018GL078607, 2018.

Dundas, V., Daae, K., and Darelius, E.: Storm-Driven Warm Inflow Toward Ice Shelf Cavities—An Idealized Study of the Southern Weddell Sea Continental Shelf System, Journal of Geophysical Research: Oceans, 129, https://doi.org/https://doi.org/10.1029/2023JC020749, 2024.

Foldvik, A., Gammelsrød, T., and Tørresen, T.: Hydrographic observations from the Weddell Sea during the Norwegian Antarctic Research Expedition 1976/77, Polar Research 3, pp. 177–193, 1985.

Foldvik, A., Gammelsrød, T., Øterhus, S., Fahrbach, E., Rohardt, G., Schröder, M., Nicholls, K. W., Padman, L., and Woodgate, R. A.: Ice shelf water overflow and bottom water formation in the southern Weddell Sea, Journal of Geophysical Research: Oceans, 109, 1–15, 410 https://doi.org/10.1029/2003jc002008, 2004.

Fretwell, P., Pritchard, H. D., Vaughan, D. G., Bamber, J. L., Barrand, N. E., Bell, R., Bianchi, C., Bingham, R. G., Blankenship, D. D., Casassa, G., Catania, G., Callens, D., Conway, H., Cook, A. J., Corr, H. F., Damaske, D., Damm, V., Ferraccioli, F., Forsberg, R., Fujita, S., Gim, Y., Gogineni, P., Griggs, J. A., Hindmarsh, R. C., Holmlund, P., Holt, J. W., Jacobel, R. W., Jenkins, A., Jokat, W., Jordan, T., King, E. C., Kohler, J., Krabill, W., Riger-Kusk, M., Langley, K. A., Leitchenkov, G., Leuschen, C., Luyendyk, B. P., Matsuoka, K., Mouginot, J., 415 Nitsche, F. O., Nogi, Y., Nost, O. A., Popov, S. V., Rignot, E., Rippin, D. M., Rivera, A., Roberts, J., Ross, N., Siegert, M. J., Smith, A. M., Steinhage, D., Studinger, M., Sun, B., Tinto, B. K., Welch, B. C., Wilson, D., Young, D. A., Xiangbin, C., and Zirizzotti, A.: Bedmap2: Improved ice bed, surface and thickness datasets for Antarctica, Cryosphere, 7, 375–393, https://doi.org/10.5194/tc-7-375-2013, 2013.

Fretwell, P., Pritchard, H., Vaughan, D., Bamber, J., Barrand, N., Bell, R. E., Bianchi, C., Bingham, R., Blankenship, D., Casassa, G., Catania, G., Callens, D., Conway, H., Cook, A., Corr, H., Damaske, D., Damn, V., Ferraccioli, F., Forsberg, R., and ... Bodart, J.: BEDMAP2 - Ice 420 thickness, bed and surface elevation for Antarctica - standardised shapefiles and geopackages (Version 1.0) [Data set], NERC EDS UK Polar Data Centre, https://doi.org/https://doi.org/10.5285/0f90d926-99ce-43c9-b536-0c7791d1728b, 2022.

Gade, H. G.: Melting of Ice Sea Water: A Primitive Model with Application to the Antarctic Ice Shelf and Icebergs, Journal of Physical Oceanography, pp. 189–198, https://doi.org/https://doi.org/10.1175/1520-0485(1979)009<0189:MOIISW>2.0.CO;2, 1979.

Gill, A. E.: Circulation and bottom water production in the Weddell Sea, Deep-Sea Research and Oceanographic Abstracts, 20, 111–140, 425 https://doi.org/10.1016/0011-7471(73)90048-X, 1973.

Hattermann, T.: Antarctic thermocline dynamics along a narrow shelf with easterly winds, Journal of Physical Oceanography, 48, 2419–2443, https://doi.org/10.1175/JPO-D-18-0064.1, 2018.

Hattermann, T., Nicholls, K. W., Hellmer, H. H., Davis, P. E. D., Janout, M., Østerhus, S., Schlosser, E., Rohardt, G., and Kanzow, T.: Observed interannual changes beneath Filchner- Ronne Ice Shelf linked to large-scale atmospheric circulation, Nature Communications, 430 12, 1–11, https://doi.org/10.1038/s41467-021-23131-x, 2021.

Hazel, J. E. and Stewart, A. L.: Are the near-Antarctic easterly winds weakening in response to enhancement of the southern annular mode?, Journal of Climate, 32, 1895–1918, https://doi.org/10.1175/JCLI-D-18-0402.1, 2019.

Hellmer, H. H., Kauker, F., Timmermann, R., Determann, J., and Rae, J.: Twenty-first-century warming of a large Antarctic ice-shelf cavity by a redirected coastal current, Nature, 485, 225–228, https://doi.org/10.1038/nature11064, 2012.

435 Hellmer, H. H., Kauker, F., Timmermann, R., and Hattermann, T.: The fate of the Southern Weddell sea continental shelf in a warming climate, Journal of Climate, 30, 4337–4350, https://doi.org/10.1175/JCLI-D-16-0420.1, 2017.

Hersbach, H., Bell, B., Berrisford, P., Horányi, A., Sabater, J. M., Nicolas, J., Radu, R., Schepers, D., Simmons, A., Soci, C., and Dee, D.: Global reanalysis: goodbye ERA-Interim, hello ERA5, ECMWF Newsletter, pp. 17–24, 2019.

Hersbach, H., Bell, B., Berrisford, P., Biavati, G., Horányi, A., Muñoz Sabater, J., Nicolas, J., Peubey, C., Radu, R., Rozum, I., Schepers, D., 440 Simmons, A., Soci, C., Dee, D., and Thépaut, J.-N.: ERA5 hourly data on single levels from 1940 to present. [Data set] (Accessed on 08-02-2023), Copernicus Climate Change Service (C3S) Climate Data Store (CDS), https://doi.org/https://doi.org/10.24381/cds.adbb2d47, 2023.

Jacobs, S. S.: On the nature and significance of the Antarctic Slope Front, Marine Chemistry, 35, 9–24, https://doi.org/10.1016/S0304-4203(09)90005-6, 1991.

445 Jacobs, S. S.: Bottom water production and its links with the thermohaline circulation, Antarctic Science, 16, 427–437, https://doi.org/10.1017/S095410200400224X, 2004.

Janout, M., Hellmer, H. H., Hattermann, T., Huhn, O., Sültenfuss, J., Østerhus, S., Stulic, L., Ryan, S., Schröder, M., and Kanzow, T.: FRIS Revisited in 2018: On the Circulation and Water Masses at the Filchner and Ronne Ice Shelves in the Southern Weddell Sea, Journal of Geophysical Research: Oceans, 126, 1–19, https://doi.org/10.1029/2021JC017269, 2021.

450 Janout, M. A., Hellmer, H. H., and Monsees, M.: Raw data of physical oceanography and current velocity data from moorings AWI252-3, AWI253-3 and AWI254-3 in Filchner Trough, February 2018 – March 2021, https://doi.org/10.1594/PANGAEA.944430, 2022.

Jensen, M. F., Fer, I., and Darelius, E.: Low frequency variability on the continental slope of the southern Weddell Sea, Journal of Geophysical Research: Oceans, 118, 4256–4272, https://doi.org/10.1002/jgrc.20309, 2013.

Lauber, J., Hattermann, T., de Steur, L., Darelius, E., Auger, M., Nøst, O. A., and Moholdt, G.: Warming beneath an East Antarctic ice shelf
455 due to increased subpolar westerlies and reduced sea ice, Nature Geoscience, https://doi.org/10.1038/s41561-023-01273-5, 2023.

Marshall, J. and Speer, K.: Closure of the meridional overturning circulation through Southern Ocean upwelling, Nature Geoscience, 5, 171–180, https://doi.org/10.1038/ngeo1391, 2012.

Martin, T., Steele, M., and Zhang, J.: Seasonality and long-term trend of Arctic Ocean surface stress in a model, Journal of Geophysical Research: Oceans, pp. 1723–1738, https://doi.org/10.1002/2013JC009425.Received, 2014.

460 Martin, T., Tsamados, M., Schroeder, D., and Feltham, D.: The impact of variable sea ice roughness on changes in Arctic Ocean surface stress: a model study, Journal of Geophysical Research: Oceans, 121, 1931–1952, https://doi.org/http://dx.doi.org/10.1002/2015JC011186, 2016.

McDougall, T. and Barker, P.: Getting started with TEOS-10 and the Gibbs Seawater (GSW) Oceanographic Toolbox, ISBN 9780646556215, 2011.

Morrison, A. K., McC. Hogg, A., England, M. H., and Spence, P.: Warm Circumpolar Deep Water transport toward Antarctica driven by
465 local dense water export in canyons, Science Advances, 6, 1–10, https://doi.org/10.1126/sciadv.aav2516, 2020.

Nicholls, K. W.: JR097 Cruise Report Autosub Under Ice Cruise to the southern Weddell Sea, https://www.bodc.ac.uk/resources/inventories/cruise_inventory/reports/jr97_05.pdf, 2005.

Nicholls, K. W., Østerhus, S., Makinson, K., Gammelsrød, T., and Fahrbach, E.: Ice-ocean processes over the continental shelf of the southern Weddell Sea, Antarctica: A review, Reviews of Geophysics, 47, https://doi.org/https://doi.org/10.1029/2007RG000250, 2009.

470 NSIDC: What are the EASE Grid., https://nsidc.org/data/ease, https://nsidc.org/data/ease, date Accessed: 2019-09-29, 2019.

NSIDC: How to convert the horizontal and vertical components to east and north, https://nsidc.org/data/user-resources/help-center/how-convert-horizontal-and-vertical-components-east-and-north, date accessed: 28 September 2024, 2024.

Orsi, A. H., Johnson, G. C., and Bullister, J. L.: Circulation, mixing, and production of Antarctic Bottom Water, Progress in Oceanography, 43, 55–109, https://doi.org/10.1016/S0079-6611(99)00004-X, 1999.

475 Østerhus, S.: Physical oceanography and current velocity data from mooring S218E, 2024.

Ryan, S., Schröder, M., Huhn, O., and Timmermann, R.: On the warm inflow at the eastern boundary of the Weddell Gyre, Deep-Sea Research Part I: Oceanographic Research Papers, 107, 70–81, https://doi.org/10.1016/j.dsr.2015.11.002, 2016.

Ryan, S., Hattermann, T., Darelius, E., and Schröder, M.: Seasonal cycle of hydrography on the eastern shelf of the Filchner Trough, Weddell Sea, Antarctica, Journal of Geophysical Research: Oceans, 122, 6437–6453, https://doi.org/10.1002/2017JC012916, 2017.

480   Semper, S. and Darelius, E.: Seasonal resonance of diurnal coastal trapped waves in the southern Weddel Sea, Antarctica, Ocean Science, 13, 77–93, https://doi.org/10.5194/os-13-77-2017, 2017.

Shchepetkin, A. F. and McWilliams, J. C.: Computational Kernel Algorithms for Fine-Scale, Multiprocess, Longtime Oceanic Simulations, Handbook of Numerical Analysis, 14, 121–183, https://doi.org/10.1016/S1570-8659(08)01202-0, 2009.

Steele, M., Zhang, J., Rothrock, D., and Stern, H.: The force balance of sea ice in a numerical model of the Arctic Ocean, Journal of
485   Geophysical Research: Oceans, 102, 21 061–21 079, https://doi.org/https://doi.org/10.1029/97JC01454, 1997.

Steiger, N. and J.-B., S.: Hydrological and current velocity data from moorings P1, P2, P4, P5 and P6 in the Filchner Trough region in the southern Weddell Sea, February 2017 to March 2021., https://doi.org/https://doi.org/10.17882/100680, 2023.

Steiger, N., Sallée, J. B., Darelius, E., Janout, M., and Østerhus, S.: Observed Pathways and Interannual Variability of the Warm Inflow Onto the Continental Shelf in the Southern Weddell Sea, Journal of Geophysical Research: Oceans, 129, e2023JC020 700,
490   https://doi.org/https://doi.org/10.1029/2023JC020700, e2023JC020700 2023JC020700, 2024.

Thompson, A. F., Stewart, A. L., Spence, P., and Heywood, K. J.: The Antarctic Slope Current in a Changing Climate, Reviews of Geophysics, 56, 741–770, https://doi.org/10.1029/2018RG000624, 2018.

Tsamados, M., Feltham, D. L., Schroeder, D., Flocco, D., Farrell, S. L., Kurtz, N., Laxon, S. W., and Bacon, S.: Impact of Variable Atmospheric and Oceanic Form Drag on Simulations of Arctic Sea Ice, Journal of Physical Oceanography, 44, 1329 – 1353,
495   https://doi.org/10.1175/JPO-D-13-0215.1, 2014.

Tschudi, M., Meier, W. N., Stewart, J. S., Fowler, C., and Maslanik, J.: Polar Pathfinder Daily 25 km EASE-Grid Sea Ice Motion Vectors, Version 4, https://doi.org/10.5067/INAWUWO7QH7B, 2019a.

Tschudi, M. A., Meier, W. N., and Stewart, J. S.: An enhancement to sea ice motion and age products, The Cryosphere Discussions, pp. 1–29, https://doi.org/10.5194/tc-2019-40, 2019b.

500   Wåhlin, A. K., Yuan, X., Bjork, G., and Nohr, C.: Inflow of Warm Circumpolar Deep Water in the Central Amundsen Shelf, Journal of Physical Oceanography, 40, 1427–1434, https://doi.org/10.1175/2010JPO4431.1, 2010.

Zhou, S., Dutrieux, P., Giulivi, C., Silvano, A., Auckland, C., Abrahamsen, P., Meredith, M., Vaňková, I., Nicholls, K., Davis, P., Østerhus, S., Gordon, A., Zappa, C., Sebaginazzi Dotto, T., Scambos, T., Gunn, K., Rintoul, S., Aoki, S., Stevens, C., Liu, C., Kim, T.-W., Lee, W. s., Janout, M., Hattermann, T., Lauber, J., Darelius, E., Wåhlin, A., Middleton, L., Castagno, P., Budillon, G., Heywood, K., Graham, J., Dye,
505   S., Hirano, D., and Miller, U. k.: Southern Ocean moored time series (south of 60°S) (OCEAN ICE D1.1), https://doi.org/10.17882/99922, 2024.